Publications of the Korean Astronomical Society
30: 417 ∼ 421, 2015 September

pISSN: 1225-1534
eISSN: 2287-6936
http://dx.doi.org/10.5303/PKAS.2015.30.2.417

NOVEL PICTURE OF THE AGN CENTRAL ENGINE ESTABLISHED BY X-RAY AND OPTICAL SIMULTANEOUS STUDIES

Hirofumi Noda
Nishina center, The institute of Physical and Chemical Research (RIKEN), Wako-shi, Saitama 351-0198, Japan
E-mail: noda@crab.riken.jp
(Received November 30, 2014; Reviced May 31, 2015; Aaccepted June 30, 2015)

ABSTRACT

We analyzed 0.5–45 keV data of NGC 3227 observed by *Suzaku* six times between 2008 October 28 and December 2. The count-count plot between the 0.5–3 keV and 3–10 keV bands exhibits a clear break, separating the data into bright and faint phases. Applying the difference spectrum method and time-averaged spectral fits to the phase data, we found the presence of two kinds of variable primary X-rays, (1) a hard primary component with $\Gamma \sim 1.7$ dominating in the faint phase and (2) a soft primary continuum with $\Gamma \sim 2.4$ appearing in the bright phase, both affected by partial absorption. Considering their timing and spectral characteristics, component (1) is presumably identical to a Compton continuum in the low/hard state, while component (2) may correspond to the hard tail emission in the high/soft state, or compact-jet emission. In that case, an accretion flow onto the central super massive black hole in NGC 3227 can be interpreted to include the two different states.

Key words: galaxies: active; X-ray: galaxies; conferences: proceedings

1. INTRODUCTION

The primary X-ray emission from the central engines of Active Galactic Nuclei (AGNs) is considered to be generated via thermal Comptonization working against black body radiation from a standard accretion disk. In many X-ray studies of AGNs, the primary spectrum has been approximated by a single Power-Law (PL) like continuum (e.g., Risaliti et al. 2004). This assumption corresponds to a picture where the Comptonizing region is single and homogeneous around the central super massive black hole (SMBH).

Under this approximation, other X-ray spectral features, deviating from the assumed single-PL spectrum, have been interpreted as secondary components, including an Fe-Kα emission line, disk- or torus-reflection component, sometimes strongly affected by relativistic effects (e.g., Miniutti et al., 2007) and/or complicated ionized absorption (e.g., Miller et al., 2008). However, the assumption for the primary X-rays has never been observationally verified, and hence, the picture of the AGN central engine is still ambiguous.

To model and independently examine primary X-ray properties without the single-PL assumption, time variability, a common property of AGNs, is the most important feature. For example, Noda et al. (2011a, b, 2013a, b, and 2014) employed a timing method utilizing count-count correlations between different energy bands, and successfully decomposed several X-ray components with different spectral and timing properties. In the present paper, we performed the often-used difference spectrum analysis to 0.5–45 keV data of the type I Seyfert NGC 3227 observed by *Suzaku*, which is broader than the energy band analyzed by Noda et al. (2014).

2. OBSERVATIONS

NGC 3227 was observed six times by *Suzaku* from 2008 October 28 to December 2, with an interval of ∼1 week. The gross and net exposures are ∼ 120 and ∼ 50 ksec, respectively. In each observation, the XIS was operated in the normal mode, and the source was located at the XIS nominal place. The data process version 2.2 was applied to all the XIS and HXD data. These data were reduced by the same method as in Noda et al. (2014).

3. LIGHT CURVES AND COUNT-COUNT PLOT

First, we extracted light curves with 20 ksec binning at 0.5–3 keV and 3–10 keV to examine the broad-band variations in the XIS band (Fig. 1). In each energy band, drastic variations on the time scale of several hours can be seen in the 1st and 3rd observation, while gradual variations on the time scale of several weeks can be seen in the other observations. In order to relate the variatons to spectral information, we created a Count-Count Plot (CCP), where ordinate and abscissa give count rates in the 0.5–3 keV and 3–10 keV band, respectively. As shown in Fig. 2, the CCP interestingly exhibits a clear break similar to the CCPs shown in Noda et al. (2014), at boundary count rates of ∼ 0.5

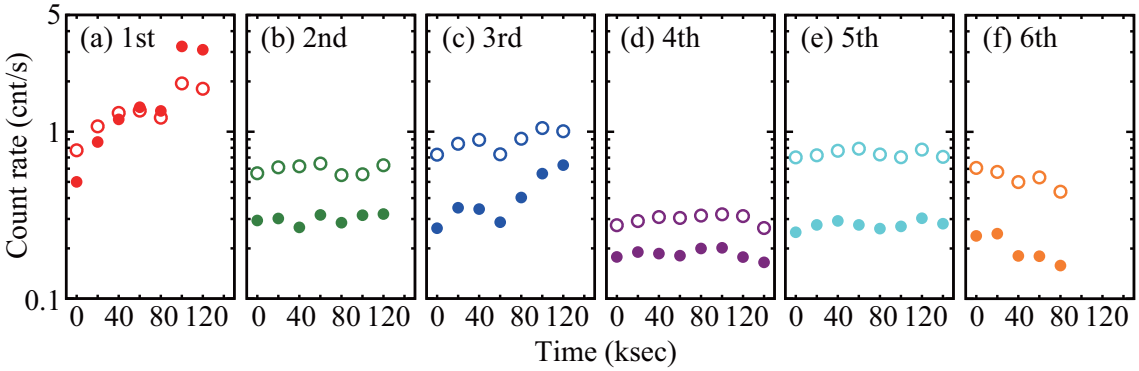

Figure 1. Light curves of 0.5–3 keV (filled circles) and 3–10 keV (open circles) band in 1st (panel a), 2nd (panel b), 3rd (panel c), 4th (panel d), 5th (panel e), and 6th (panel f) observation. All the bin sizes are 20 ksec, and errors are omitted because they all are within the circles.

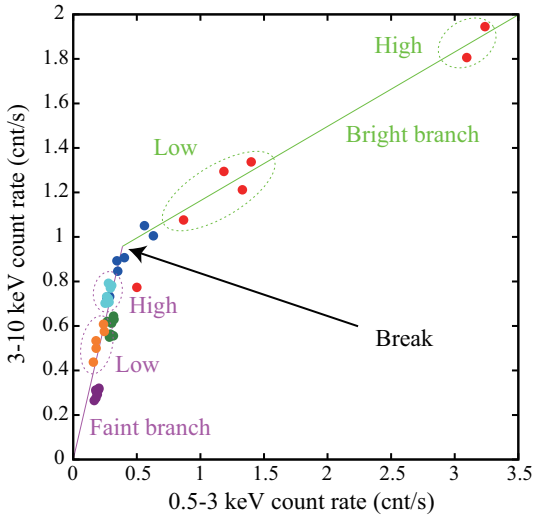

Figure 2. A count-count plot between count rates of 0.5–3 keV and 3–10 keV band binned into 20 ksec. Colors represent the same observations as those in Fig. 1. Errors are omitted as well as the light curves. The data used to extract difference spectra in the Faint and Bright branch are shown in purple and green dotted circle, respectively.

cnt s^{-1} in the 0.5–3 keV band and $\sim$ 1 cnt s^{-1} in the 3–10 keV band (hence, $\sim$ 1.5 cnt s^{-1} in the 0.5–10 keV band).

The distribution of data points is seemingly a straight line, above and below the boundary count rate, showing that the spectral shapes did not change approximately in the lines, while drastically changing at the boundary. Hereafter, we call the data distributions above and below the boundary, the Bright and Faint branch, respectively, for convenience, after Noda et al. (2014). It should be noted that not only the spectral shapes but also the timescale of the variations are significantly different between the Faint (on $\sim$ weeks) and Bright (on $\sim$ hours) branch. This means that the CCP break cannot be explained by absorption changes, because an absorption cannot affect the timescales of flux variations. Therefore, it is most natural to consider the presence of two types of variable continua, with the CCP break possibly due to an alternation between them.

4. DIFFERENCE SPECTRUM ANALYSIS

To examine spectral shapes of the variable components in the Bright and Faint branch, we employed a traditional timing analysis, called the difference spectrum method, which is often applied in AGN X-ray studies. In the Faint branch, the average count rate in the 0.5–10 keV band is $\sim$ 0.8 cnt s^{-1}, and the count rates in the 5th and 6th observations are higher and lower than the average, respectively. Then, we extracted a Faint-high spectrum in the 0.5–45 keV band from the 5th dataset, and a Faint-low one from 6th dataset, and subtracted the latter from the former to derive a difference spectrum in the Faint branch. As shown in Fig. 3(a), the Faint-branch difference spectrum is relatively hard, and concave in the $\sim$ 0.5–3 keV band. This is a typical feature of partial absorption, so we fitted it with a partially-absorbed PL model, `pcfabs * cutoffpl` in XSPEC12. In the fit, the cutoff energy $E_{\rm cut}$ was fixed at 200 keV, while the the column density $N_{\rm H}$ and covering fraction $f_{\rm cvr}$ of the partial absorption, the photon index Γ and the normalization $N_{\rm PL}$ of the PL were left free. The resulting fit had χ^2/dof=104.63/94, giving $N_{\rm H} \sim 5.0^{+0.55}_{-0.59}$ cm^{-2}, $f_{\rm cvr} \sim 0.95 \pm 0.01$, and $\Gamma \sim 1.73^{+0.07}_{-0.14}$.

To apply the difference spectrum analysis to the Bright branch, we divided, as shown in Fig. 2, the data into a Bright-high and Bright-low phase with count rates are above and below an average count rate of $\sim$ 3.1 cnt s^{-1} in the 0.5–10 keV band, respectively. Then, we extracted a spectrum in each phase, and subtracted a Bright-low spectrum from the Bright-high one. As a result, a 0.5–45 keV difference spectrum in the Bright branch was found to be relatively soft and also concave in the 0.5–3 keV band, as shown in Fig. 3(a). Fitting with the same model as that used for the Faint-branch difference spectrum, the result became acceptable with χ^2/dof=69.30/64, giving $N_{\rm H} \sim 0.8 \pm 0.1$ cm^{-2}, $f_{\rm cvr} \sim 0.76^{+0.02}_{-0.03}$, and $\Gamma \sim 2.24 \pm 0.06$, which were all significantly different from those in the Faint branch. Therefore, we successfully discovered, by the reliable timing method, two distinct types of variable components, the hard and soft X-ray continua.

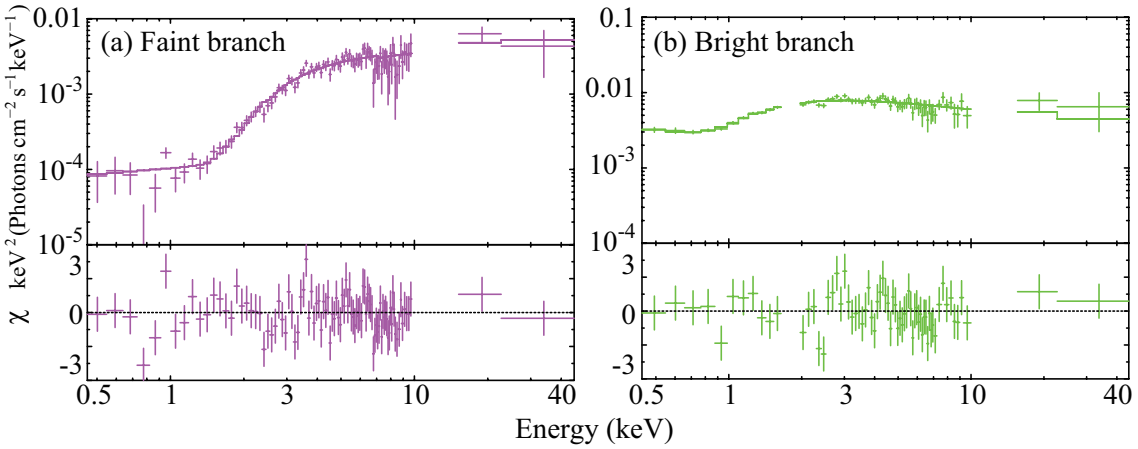

Figure 3. Difference spectra in a νF_ν form derived in the Faint (panel a) and the Bright (panel b) branch.

5. TIME-AVERAGED SPECTRUM ANALYSIS

To compare spectral components in the Faint and Bright branch, we finally move to time-averaged spectral fits, taking the two kinds of variable continua obtained in §4 into account. In the Faint branch, the 0.5–10 keV count rate in the 6th dataset is the closest to the average of the Faint-branch datasets. Hence, we analyzed the time-averaged spectrum in the 6th observation. Because the variable component in the Faint branch was found to be a partially-absorbed hard PL in §4, we utilized the model of `pcfabs1 * cutoffpl1 + gsmooth * pexmon`, where `pcfabs1 * cutoffpl1` is for a partially-absorbed PL as in §4, while `gsmooth * pexmon` is for a disk- or torus-reflection component with a weakly-smeared Fe-Kα, β, and Ni-Kα emission lines in XSPEC12. In the `pcfabs1 * cutoffpl1` model, the free and fixed parameters were same as those in §4. In the `gsmooth * pexmon` model, the photon index of the incident PL, cutoff energy, reflection fraction, abundance, and the inclination angle were fixed at 2, 200 keV, 1, 1 Solar, and 60°, respectively, while the normalization was left free. As a result, the fit became almost successful with χ^2/dof=173.90/121, as shown in Fig. 3(a) and Table 1. Thus, the Faint-branch time-averaged spectrum is possibly reproduced just with the hard continuum and the reflection component.

Can the Bright-branch time-averaged spectrum be explained by the same model as that for the Faint-branch one? To examine this, we fitted the time-averaged spectrum in the 1st observation with the same model fitted to the 6th dataset. However, the fit was unsuccessful with χ^2/dof=891.42/461, mainly because of large residuals in the 0.5–2 keV band. These residuals required an additional soft continuum. Then, we added another partially-absorbed PL model, which corresponds to the soft variable continuum derived from the difference spectrum in the Bright branch in §4, and again fitted with the model of `pcfabs1 * cutoffpl1 + pcfabs2 * cuotffpl2 + gsmooth * pexmon`. The fixed and free parameters in the `pcfabs2 * cutoffpl2` model were the same as those in `pcfabs1 * cutoffpl1`. As a result, the fit was significantly improved with χ^2/dof=632.39/457, which is still unacceptable, mainly due to residuals of fine absorption lines by ionized oxygen and iron at $\sim$ 0.8 keV and $\sim$ 7 keV, respectively. Therefore, we added ionized absorption effects modeled by `zxipcf` and two negative gaussians corresponding to ionized absorption lines. (For more details, see Noda et al. 2014.) Finally, we derived an almost successful result with χ^2/dof=538.74/450, as shown in Fig. 3(b), giving the parameter values summarized in Table 1. Therefore, the 0.5–45 keV time-averaged spectrum in the Bright branch was found to be reproduced with both hard and soft variable continua, while that in the Faint branch with only the hard variable component, in addition to the disk- or torus-reflection component.

Table 1
PARAMETERS DERIVED IN THE FITS TO THE TIME-AVERAGED SPECTRA.

Main comp.		Faint	Bright
`pcfabs1`	$N_{\rm H1}^{\rm a}$	8.2 ± 0.4	$5.5^{+1.4}_{-1.1}$
	$f_{\rm cvr1}$	0.87 ± 0.01	$0.95^{+0.05}_{-0.17}$
`cutoffpl1`	Γ_1	1.40 ± 0.05	1.39 ± 0.05
	$E_{\rm cut}$ (keV)	200 (fix)	
	$N_{\rm PL1}^{\rm b}$	0.30 ± 0.03	$0.37^{+0.01}_{-0.02}$
`pcfabs2`	$N_{\rm H2}^{\rm a}$	–	1.0 ± 0.1
	$f_{\rm cvr2}$	–	$0.80^{+0.08}_{-0.03}$
`cutoffpl2`	Γ_2	–	$2.26^{+0.25}_{-0.13}$
	$E_{\rm cut}$ (keV)	–	200 (fix)
	$N_{\rm PL2}^{\rm b}$	–	$1.24^{+0.18}_{-0.09}$
`pexmon`	$\Gamma_{\rm ref}$	2 (fix)	
	$E_{\rm cut}$ (keV)	200 (fix)	
	$f_{\rm ref}$	1 (fix)	
	z	0.00386 (fix)	
	A ($Z_\odot$)	1 (fix)	
	$A_{\rm Fe}$ ($Z_{\rm Fe,\odot}$)	1 (fix)	
	i (degree)	60 (fix)	
	$N_{\rm ref}^{\rm b}$	1.14 ± 0.13	1.15
χ^2/d.o.f.		173.90/121	538.74/450

[a] Equivalent hydrogen column density in 10^{22} cm^{-2}.
[b] The PL and reflection normalization at 1 keV, in units of 10^{-2} photons keV^{-1} cm^{-2} s^{-1} at 1 keV.

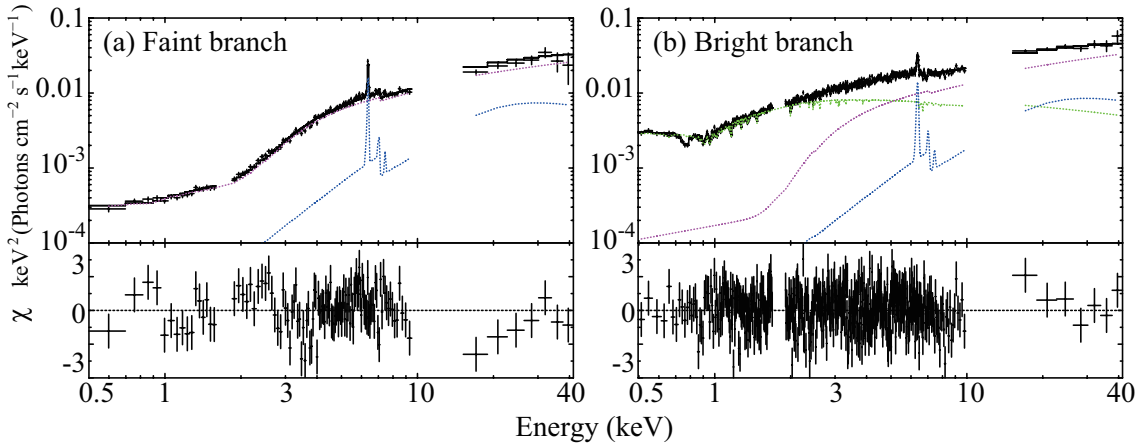

Figure 4. Results of the fits to time-averaged spectra in a νF_ν form in the Faint (panel a) and the Bright branch (panel b).

6. SUMMARY AND DISCUSSION

By the difference spectrum method (§4) and time-averaged spectral analyses (§5), we confirmed the presence of the two variable components in the 0.5–45 keV band, summarized below.

- A hard spectral component with $\Gamma \sim 1.7$, affected by partial absorption with a column density of $\sim 10^{23}$ cm^{-2}. It dominates when the source is faint and the 0.5–10 keV count rate below 1.5 cnt s^{-1}, and varies on the timescale of $\sim$ weeks.
- A soft continuum which has a $\Gamma \sim 2.4$ spectrum, partially absorbed by neutral matter with $N_{\rm H} \sim 10^{22}$ cm^{-2}. This component appears when the source is bright and the 0.5–10 keV count rate above 1.5 cnt s^{-1}, in addition to the hard variable component. Its variation is on the timescale of $\sim$ hours.

Both variable emissions should be primary X-rays, because they appeared and varied in flux independently of each other. This means that the primary X-ray emission from an AGN is not a single PL, as approximated in many previous studies.

How are the two kinds of primary X-rays radiated? Taking the spectral and timing characteristics into account, the hard primary X-rays presumably correspond to a Comptonization emission generated in a radiatively inefficient accretion flow formed in the low/hard state (e.g., Yuan & Narayan, 2014), because it dominates at a lower accretion rate. On the other hand, the soft spectrum, fast variability and the emergence with a high accretion rate of the soft primary X-rays may be related to a hard tail emission created by a standard disk in the high/soft state (e.g., Remillard & McClintock, 2006), or a compact-jet emission (e.g., Ghisellini et al., 2004). Therefore, the X-ray spectrum of NGC 3227 can be interpreted as the mixture of the two different states, and the CCP break possibly represents a kind of state transition for an accretion flow onto a SMBH.

Since the spectral shape and time variability are significantly different between the hard and soft primary X-rays, their generating regions might be geometrically separated, as shown in Noda et al. (2014). In that case, the correlation of flux variation with optical/UV should be distinct between the hard and soft primary components. Because a standard accretion disk radiates optical/UV via black body radiation, one well correlated with the optical/UV would be expected to have a generating region closer to the disk, while the origin of the other is presumably farther from the disk. Thus, we can study the geometry of the AGN central engine by X-ray and optical/UV simultaneous monitoring. Based on this idea, we are now performing simultaneous observations of X-ray and optical emission of a bright type I Seyfert NGC 3516 with *Suzaku* and several ground based Japanese telescopes. After decomposing the primary X-rays by the timing analyses, we can examine the correlation between flux variations of each primary X-ray and optical/UV signal. The results of these monitors will be reported elsewhere.

REFERENCES

Ghisellini, G., Haardt, F., & Matt, G., 2004, Aborted Jets and the X-ray Emission of Radsio-quiet AGNs, A&A, 413, 535

Miller, L., Turner, T. J., & Reeves, J. N., 2008, An Absorption Origin for the X-ray Spectral Variability of MCG–6-30-15, A&A, 483, 437

Miniutti, G., Fabian, A. C., & Anabuki, N., et al., 2007, *Suzaku* Observations of the Hard X-Ray Variability of MCG–6-30-15: the Effects of Strong Gravity around a Kerr Black Hole, PASJ, 59, S315

Noda, H., Makishima, K., & Yamada, S., et al., 2014, *Suzaku* Studies of the Central Engine in the Typical Type I Seyfert NGC 3227: Detection of Multiple Primary X-Ray Continua with Distinct Properties, ApJ, 794, 2

Noda, H., Makishima, K., Nakazawa, K., & Yamada, S., 2013a, A *Suzaku* Discovery of a Slowly Varying Hard X-Ray Continuum from the Type I Seyfert Galaxy NGC 3516, ApJ, 771, 100

Noda, H., Makishima, K., Nakazawa, K., et al., 2013b, The Nature of Stable Soft X-Ray Emissions in Several Types of Active Galactic Nuclei Observed by *Suzaku*, PASJ, 65,4

Noda, H., Makishima, K., Yamada, S., et al., 2011a, *Suzaku* Studies of Wide-Band Spectral Variability of the Bright Type I Seyfert Galaxy Markarian 509, PASJ, 63, 925

Noda, H., Makishima, K., Uehara, Y., Yamada, S., & Nakazawa, K., 2011b, *Suzaku* Discovery of a Hard Com-

ponent Varying Independently of the Power-Law Emission in MCG–6-30-15, PASJ, 63, 449
Remillard, R. A., & McClintock, J. E., 2006, X-Ray Properties of Black-Hole Binaries, ARA&A, 44, 49
Risaliti, G., & Elvis, M., 2004, Supermassive Black Holes in the Distant Universe, 308, 187
Yuan, F., & Narayan, R., 2014, Hot Accretion Flows Around Black Holes, ARA&A, 52, 529